Analysis and Development of Millimeter-Wave Waveguide-Junction Circulator with a Ferrite Sphere

Edward Kai-Ning Yung, *Senior Member, IEEE*, Ru Shan Chen, *Member, IEEE*, Ke Wu, *Senior Member, IEEE*, and Dao Xiang Wang

***Abstract*—This paper presents a class of new easy-to-fabricate ferrite–sphere-based waveguide Y-junction circulators for potentially low-cost millimeter-wave applications. A new three-dimensional modeling strategy using a self-inconsistent mixed-coordinates-based modal field-matching procedure is developed to characterize electrical performance of the proposed circulator. It is found that the circulating mechanism of the ferrite–sphere post is different from its full-height ferrite counterpart in that the new structure operates in a turnstile fashion with resonant characteristics, while the conventional device operates on a transmission cavity model. Extensive comparable studies between the new and conventional circulators are made to show that the electrical behaviors of the new structure are also distinct and radial power-density profiles are not stationary, as in the case of the full-height ferrite post circulator for different geometrical parameters. Results obtained by the analysis technique are compared with the available results for a full/partial-height ferrite circulator, showing an excellent agreement. Our calculated and measured results are also presented for W-band circulators with the proposed ferrite–sphere technique, indicating some interesting characteristics such as the frequency offset behavior of the isolation and reflection curves. In addition, radial power-density profiles are plotted inside and outside the ferrite sphere to illustrate its intrinsic circulating mechanism, as well as its difference, as compared to its full-height ferrite structure.**

***Index Terms*—Ferrite device, junction circulator, millimeter-wave, mode-matching technique.**

I. Introduction

THE H-plane waveguide Y-junction circulator has been extensively used in microwave and millimeter-wave systems. The most popular anisotropic building block used to guide signal waves in circulation is a ferrite cylindrical post of full or partial waveguide height. In addition, other forms, e.g., triangular and hexagonal post, may also be designed in a similar way for the circulator use. As the operating frequency goes up into millimeter-wave range, such a junction circulator becomes proportionally small in size. Since the relative ferrite permittivity is usually high (>10), the diameter of a ferrite cylinder can be of the order of 1 mm, e.g., operating in the W-band. To enhance the manufacturing repeatability, a relatively large dimension is desired, and it can be achieved through the use of a higher order mode operation. However, it leads to an unfortunately higher ferrite loss. The miniaturization and hardness of the ferrite post are expected to bring about an expensive craftsmanship in mounting it into the equally tiny waveguide junction.

To address the above-described challenging issues, an innovative idea was contemplated [1]. In essence, it is to replace the ferrite cylinder simply by a ferrite sphere. This is because the ferrite sphere can be easily handled as if there were ball bearings. As miniaturized ball bearings of 1-mm diameter or even less have been micromachined for decades, it can be said that the large-scale production techniques are quite matured. In addition, a sphere is always normal to the metallic floor of the waveguide junction, and the surface-mounting technique is much less involved. Nevertheless, the modeling and accurate analysis of a circulator made of this kind of ferrite sphere becomes very difficult because of a spherical topology that is not consistent with the waveguide coordinate.

The analysis of a waveguide Y-junction circulator was first carried out by Davis [2], whose technique was later extended to the modeling of a class of complicated structures such as a junction with a centrally pinned full-height ferrite post or a composite ferrite post. A number of techniques [3]–[7] were then proposed to model the waveguide-junction circulators having a full-height ferrite post with arbitrary shape. Even though they are general, these analyses are limited to the circulators with a full-height ferrite post. As for the circulator designed with a partial-height ferrite post, Owen [8] demonstrated that it operates in a turnstile fashion with rotating modes guided along the ferrite axis. It also has a wider bandwidth, as compared to its full-height counterpart. Although a number of approximate formulas have been given for engineering design [9]–[11], there is the lack of a rigorous theoretical model considering the realistic boundary conditions [12]–[18]. The analysis of a waveguide-junction circulator with a partial-height ferrite post was presented for E-plane

Manuscript received September 9, 1997. This work was supported by the Research Grant Council, Government of Hong Kong, under a Competitive Earmarked Research Grant.

E. K.-N. Yung, R. S. Chen, and D. X. Wang are with the Wireless Communication Research Center, Department of Electronic Engineering, City University of Hong Kong, Kowloon, Hong Kong.

K. Wu is with the Polygrames Research Center, Department of Electrical and Computer Engineering, Ecole Polyetchnique, Montréal, P.Q., Canada H3C 3A7.

Publisher Item Identifier S 0018-9480(98)08004-1.

by Shandwily [13] and for H-plane by Akaiwa [14] on the basis of simplified field expressions proposed by Hauth [12]. Both volume and surface modes were used as eigenmodes to expand electromagnetic fields in a ferrite post by Dou [15], [16]. His analysis indicated $n = 2$ Chebyshev response related characteristics, as observed in his experiments. Nevertheless, the analyses are still restricted to the case of a partial-height ferrite post.

In our case, the permeability tensor and spherical coordinate make it impossible to find a closed-form analytical expression of fields inside a magnetized ferrite sphere. The self-inconsistent three coordinates (rectangular, cylindrical, and spherical) involved in a Y-junction waveguide circulator with a ferrite sphere give rise to an additional difficulty in handling its boundary condition in the analysis. Although a technique that is based on the equivalent principle and cavity field expansion [17], [18] was proposed to model a waveguide junction having an arbitrarily shaped anisotropic medium, hundreds of expanded functions are required to achieve only less than 3% error in their full-height composite ferrite-post circulators. Complete discrete-domain-based techniques such as finite-difference and finite-element methods [6] are usually computationally deficient because of the three involved different coordinates-related boundary conditions, as well as the anisotropic medium. Therefore, an outlook into the development of a new technique is motivated. This technique should effectively combine the advantageous features of both analytical and numerical algorithms. In this paper, the mode-matching technique and the method of moments are jointly used to model the H-plane millimeter-wave Y-junction circulator with a ferrite sphere.

In Section II, the ferrite sphere is first approximated by bodies of revolution with segmented cross sections [19], [20], whose surface is circumscribed by the spherical surface. The whole region in the Y-junction can be regarded as a composition of many annulus, i.e., concentrically cascaded conducting parallel-plate cylindrical waveguides loaded with multiple layers containing dielectric (air) and ferrite medium in series. In each annulus (parallel-plate cylindrical waveguide), field profiles of each region partially filled with different medium can be expanded through eigenmodes. The continuity of tangential electric and magnetic fields at the interface of two adjacent regions of the dielectric and ferrite is reinforced to obtain a solution for the radial propagation constant in the two regions in question. Matching tangential fields along every interfacial plane and applying the Galerkin technique lead to a set of solvable linear equations. Results are presented in Section III, showing that our analysis is in good agreement with the available results for the limiting case (full-height ferrite-post circulator). Our calculated center operating frequency is 3.81% lower than the experiments. The predicted insertion loss and isolation are in fairly good agreement with the measured results, considering the fact that the ferrite loss is neglected in the model. The radial power-density profile versus the orientation, as well as the complete power-density profile versus the position over the Y-junction, are also plotted so that the operating mechanism of the ferrite sphere can be better understood as to its function of circulating signal waves. These results and discussion indicate the validity of our analysis and also that the ferrite sphere is an efficient alternative in the design of a quality circulator for millimeter-wave applications.

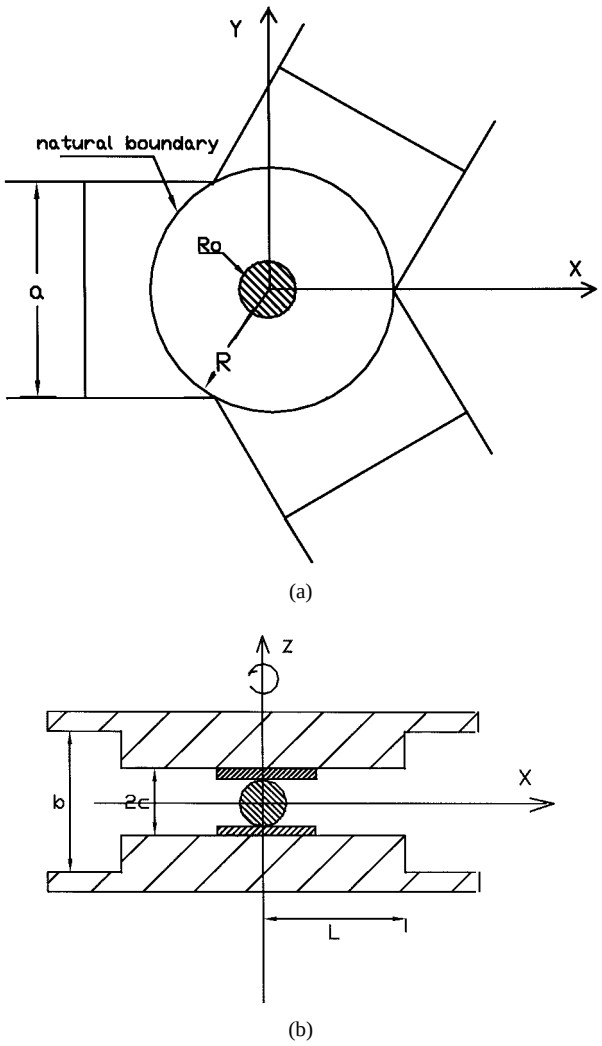

Fig. 1. Schematic diagrams of an H-plane Y-junction waveguide circulator with the proposed ferrite sphere. (a) Top view of the Y-junction. (b) Side view of the junction.

II. Field-Based Model of Y-Junction Circulator with a Ferrite Sphere

As shown in Fig. 1, the H-plane Y-junction circulator with a ferrite sphere presents a symmetry at the $z = 0$ plane, and the symmetric plane can be considered as an electric wall, which allows us to model either side for the whole structure. The junction can be divided into such regions as a series of concentrically cascaded conducting parallel-plate cylindrical waveguides loaded with dielectric (air) and ferrite media. In each loaded waveguide, the ferrite is denoted as region I, the dielectric as region II, and the dielectric (air) exists only for the outermost region. With field expansion in each region, the field-matching procedure is first made between different media (regions I and II), defined in each concentrically cylindrical layer, assuming the same radial propagation constant for the two regions. The similar field matching is then applied to

neighboring concentrically cylindrical layers. In this way, a set of linear equations can be set up by matching tangential fields in each interfacial plane. Results are easily obtained from solving these linear equations.

A. Field Expression in the Y-Junction Regions

First of all, the circulator structures are supposed to be lossless and the ferrite sphere is homogeneously magnetized in the z-direction by an externally applied bias field H_o^e. The biasing range includes the partially magnetized and demagnetized state ($H_o^e = 0$), which is particularly useful for below-resonance circulators. The longitudinally magnetized (z) field equations are formulated as follows:

$$\begin{aligned}\nabla\times\vec{E}&=-j\omega\mu_o[\mu]\vec{H}\\ \nabla\times\vec{H}&=j\omega\epsilon_o\epsilon_f\vec{E}\\ \nabla\cdot\vec{E}&=0\\ \nabla\cdot\vec{B}&=0\end{aligned}\tag{1}$$

in which

$$[\mu]=\begin{bmatrix}\mu & -j\kappa & 0\\ j\kappa & \mu & 0\\ 0 & 0 & \mu_z\end{bmatrix}$$

if the magnetization is saturated with $\mu_z = 1$ and the tensor elements are defined in a similar manner as in [1]. The development of the above equations leads to (2) and (3), shown at the bottom of this page, where ϵ_f is the relative permittivity of the ferrite sphere and $K_f^2 = \omega^2\epsilon_o\mu_o\epsilon_f$, $\mu_{\text{eff}} = \mu_e = (\mu^2 - \kappa^2/\mu)$. Now, through a simple variable separation procedure $H_z = T(r,\varphi)Z_H(z)$, $E_z = T(r,\varphi)Z_E(z)$ under a prescribed condition of $\nabla_t^2 T + K_c^2 T = 0$, (2) can be reformulated as

$$\begin{aligned}(K_f^2\mu - K_c^2)Z_H + \frac{\mu_z\partial^2 Z_H}{\mu\partial z^2} + \frac{\omega\epsilon_o\epsilon_f\kappa}{\mu}\frac{\partial Z_E}{\partial z} &= 0\\ (K_f^2\mu_e - K_c^2)Z_E + \frac{\partial^2 Z_E}{\partial z^2} - \frac{\omega\mu_o\kappa\mu_z}{\mu}\frac{\partial Z_H}{\partial z} &= 0\end{aligned}\tag{4}$$

where K_c is radial propagation constant in the ferrite medium.

Such above equations can be easily arranged into a fourth-order homogeneous linear differential equation as follows:

$$\frac{\partial^4 Z_E}{\partial z^4} + \left[2K_f^2\mu - K_c^2\left(1+\frac{\mu}{\mu_z}\right)\right]\cdot\frac{\partial^2 Z_E}{\partial z^2} + \frac{\mu}{\mu_z}(K_f^2\mu_z - K_c^2)(K_f^2\mu_e - K_c^2)Z_E = 0.\tag{5}$$

A similar equation can be also obtained for Z_H. The expected solution can be obtained from roots of these characteristic equations.

1) Field Formulation in the Ferrite Region: It is now easy to derive the related field formulation in the ferrite region from the above basic equations as follows:

$$\begin{aligned}E_{zF} &= \sum_{i=1}^{2}\sum_{n=-\infty}^{+\infty}\sum_{l=1}^{2} A_{inl}\cos\beta_i z R_{nl}(K_c r)e^{jn\varphi}\\ H_{zF} &= \sum_{i=1}^{2}\sum_{n=-\infty}^{+\infty}\sum_{l=1}^{2}\frac{\beta_i}{\omega\mu_0}t_i A_{inl}\sin\beta_i z R_{nl}(K_c r)e^{jn\varphi}\\ E_{\varphi F} &= \sum_{i=1}^{2}\sum_{n=-\infty}^{+\infty}\sum_{l=1}^{2} jA_{inl}\frac{K_c\beta_i}{K_f^2}\\ &\quad\cdot\left[q_i R'_{nl}(K_c r) - P_i\frac{nR_{nl}(K_c r)}{K_c r}\right]\sin\beta_i z e^{jn\varphi}\\ H_{\varphi F} &= \sum_{i=1}^{2}\sum_{n=-\infty}^{+\infty}\sum_{l=1}^{2} -j\frac{K_c}{\omega\mu_0}A_{inl}\\ &\quad\cdot\left[P_i R'_{nl}(K_c r) - r_i\frac{nR_{nl}(K_c r)}{K_c r}\right]\cos\beta_i z e^{jn\varphi}\end{aligned}\tag{6}$$

with

$$R_{n1}(K_c r) = \begin{cases} J_n(K_c r), & K_c^2 > 0\\ I_n(K_c r), & K_c^2 < 0\end{cases}$$

and

$$R_{n2}(K_c r) = \begin{cases} Y_n(K_c r), & K_c^2 > 0\\ K_n(K_c r), & K_c^2 < 0\end{cases}$$

as well as

$$\begin{aligned}\beta_{1,2}^2 &= K_f^2\mu - K_c^2\frac{\mu+\mu_z}{2\mu}\\ &\quad\pm\left[K_c^4\left(\frac{\mu-\mu_z}{2\mu_z}\right)^2 + \frac{\kappa^2}{\mu_z}K_f^2(K_f^2\mu_z - K_c^2)\right]^{1/2}\\ P_i &= K_f^2/K_c^2\\ t_i &= (\omega\epsilon_0\epsilon_f\kappa\beta_i)/(K_f^2\mu - K_c^2\mu - \beta_i^2)\\ q_i &= \mu_z t_i P_i\\ r_i &= ((K_f^2\mu - K_c^2 - \beta_i^2)/(\kappa K_c^2)\end{aligned}$$

in which J_n, Y_n, I_n, and K_n are the nth-order Bessel functions of the first and second kinds, as well as the modified first and second kinds, respectively. The constants associated with the second-kind Bessel functions Y_n, K_n will be zero for the inner layer.

$$\begin{aligned}\nabla_t^2 H_z + \frac{\mu_z}{\mu}\frac{\partial^2 H_z}{\partial z^2} + K_f^2 H_z\mu_z + \frac{\omega\epsilon_0\epsilon_f\kappa}{\mu}\frac{\partial E_z}{\partial z} &= 0\\ \nabla_t^2 E_z + \frac{\partial^2 E_z}{\partial z^2} + K_f^2\mu_{\text{eff}}E_z - \frac{\omega\mu_o\kappa}{\mu}\frac{\partial H_z}{\partial z} &= 0\end{aligned}\tag{2}$$

$$\left[\frac{\partial^2}{\partial z^2} + K_f^2\mu\right]E_t + j\kappa K_f^2\hat{z}\times E_t = \nabla_t\frac{\partial E_z}{\partial z} + j\omega\mu_o\hat{z}\times\nabla_t H_z + \omega\mu_o\kappa\nabla_t H_z$$

$$\left[\frac{\partial}{\partial z^2} + K_f^2\mu\right]H_t + j\kappa K_f^2\hat{z}\times H_t = \nabla_t\frac{\partial E_z}{\partial z} - j\omega\mu\epsilon\hat{z}\times\nabla_t E_z\tag{3}$$

2) Field Formulation in the Dielectric Region: To characterize the dielectric region is to substitute the above related field equations by its characteristic dielectric elements such as $\kappa = 0$, $\epsilon_f = \epsilon_d$, and $\mu = 1$, shown in (7), at the bottom of this page, with

$$R_{nl}(K_c r) = \begin{cases} J_n(K_c r), & K_c^2 > 0 \\ I_n(K_c r), & K_c^2 < 0 \end{cases}$$
$$R_{n2}(K_c r) = \begin{cases} N_n(K_c r), & K_c^2 > 0 \\ K_n(K_c r), & K_c^2 < 0 \end{cases}$$

as well as

$$R'_{nl}(K_c r) = \partial R_{nl}(K_c r)/\partial r,$$
$$K_z^2 = \omega^2 \epsilon \mu_o - K_c^2$$
$$\epsilon = \epsilon_0 \epsilon_d.$$

3) Field Formulation in the Cylindrical Parallel-Plate Waveguide: As for the air-filled cylindrical parallel-plate waveguide, which surrounds the ferrite and dielectric layers in the junction, the field expressions are formulated as (8), shown at the bottom of this page, with $K_a^2 = (m\pi/c)^2 - K_0^2$, $K_0^2 = \omega^2 \epsilon_0 \mu_0$, $Y_o = \sqrt{\epsilon_o/\mu_o}$, $\beta_m = (m\pi/c)$, $m = 1, 2, \cdots, M$.

B. Interfacial Matching of Tangential-Field Components

There are four distinct types of boundary interfaces. The first is related to the interface of ferrite and dielectric media in each annulus, as indicated in Fig. 2. The radial propagation constant K_c can be obtained as long as this matching procedure is completed. In addition, fields of the dielectric region in each annulus can also be calculated by the fields in the ferrite region. The second type is the interface between two adjacent annuli. There will be exactly $J-1$ interfaces if J annuli are considered. The tangential-field matching leads to the fields of an interface that can be calculated from its subsequent (or neighboring) one. In this way, the same matching procedure is repeated until fields of the last annulus are calculated from the fields of the first one. The third type is concerned with the interface between the last annulus (say, the Jth annulus) and the outer dielectric (air or a surrounding dielectric) region, while the fourth type is in relation to the natural boundary ($r = 1/\sqrt{3}$, a is the width of rectangular waveguides) between the three rectangular waveguide arms and Y-junction region. The field matching related to this boundary has been discussed in [3] and [4].

$$E_{zD} = \sum_{l=1}^{2} \sum_{n=-\infty}^{+\infty} B_{\mathrm{ln}l} R_{nl}(K_c r) \cos K_z(c-z) e^{jn\varphi}$$
$$H_{zD} = \sum_{l=1}^{2} \sum_{n=-\infty}^{+\infty} B_{2nl} R_{nl}(K_c r) \sin K_z(c-z) e^{jn\varphi}$$
$$E_{\varphi D} = j \sum_{l=1}^{2} \sum_{n=-\infty}^{+\infty} \left\{ B_{\mathrm{ln}l} \frac{nK_z}{K_c^2 r} R_{nl}(K_c r) + B_{2nl} \frac{\omega \mu_o}{K_c} R'_{nl}(K_c r) \right\} \sin K_z(c-z) e^{jn\varphi}$$
$$H_{\varphi D} = -j \sum_{l=1}^{2} \sum_{n=-\infty}^{+\infty} \left\{ B_{\mathrm{ln}l} \frac{\omega \epsilon}{K_c^2} R'_{nl}(K_c r) + B_{2nl} \frac{K_z n}{K_c^2 r} R_{nl}(K_c r) \right\} \cos K_z(c-z) e^{jn\varphi} \tag{7}$$

$$E_z^{\mathrm{air}} = \sum_{n=-\infty}^{+\infty} \left\{ C_{1no} J_n(K_0 r) + C_{2no} Y_n(K_0 r) + \sum_{m=1}^{\infty} [C_{1\mathrm{nm}} I_n(K_a r) + C_{2\mathrm{nm}} K_n(K_a r)] \cos \beta_m z \right\} e^{jn\varphi}$$
$$H_z^{\mathrm{air}} = \sum_{n=-\infty}^{+\infty} \sum_{m=1}^{\infty} \{ D_{1\mathrm{nm}} I_n(K_a r) + D_{2mn} K_n(K_a r) \} \sin \beta_m z e^{jn\varphi}$$
$$E_\varphi^{\mathrm{air}} = \sum_{n=-\infty}^{+\infty} \sum_{m=1}^{\infty} \left\{ \frac{m\pi}{K_a^2 c} \frac{n}{4} [C_{1\mathrm{nm}} I_n(K_a r) + C_{2\mathrm{nm}} K_n(K_a r)] + \frac{\omega \mu_0}{K_a} [D_{1\mathrm{nm}} I'_n(K_a r) + D_{2\mathrm{nm}} K'_n(K_a r)] \right\} \sin \beta_m z e^{jn\varphi}$$
$$H_\varphi^{\mathrm{air}} = \sum_{n=-\infty}^{+\infty} j \left\{ -Y_o [C_{1no} J'_n(K_o r) + C_{2no} Y'_n(K_0 r)] + \sum_{m=1}^{\infty} \left[\frac{\omega \epsilon_0}{K_a} [C_{1\mathrm{nm}} I'_n(K_a r) + C_{2\mathrm{nm}} K'_n(K_a r)] \right. \right.$$
$$\left. \left. - \frac{jm\pi}{K_a^2 c} \frac{n}{r} [D_{1\mathrm{nm}} I_n(K_a r) + D_{2\mathrm{nm}} K_n(K_a r)] \right] \right\} \cos \beta_m z e^{jn\varphi} \tag{8}$$

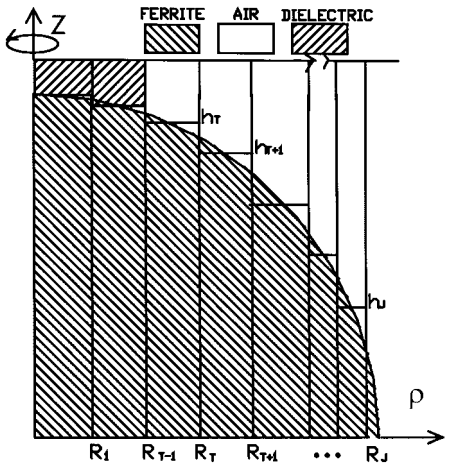

Fig. 2. Piecewise segmentation of a ferrite sphere loaded H-plane Y-junction in terms of a number of concentrically cascaded cylindrical parallel-plate waveguides loaded by ferrite and dielectric media.

1) Field Matching of Ferrite and Dielectric Region in Each Annulus: Now that the tangential-field components are matched at the interface of the dielectric and ferrite layer with the continuity condition, it is used to obtain the radial propagation constant and also derive the constants B_{1n1}, B_{2n1} in terms of A_{1n1} and A_{2n1}. The resulting equations are arranged in such a way that each B_n is characterized by A_n and also a set of four homogeneous equations. Matching the tangential fields at $z = h$ yields a complex coefficient transcendental equation, such that

$$\begin{aligned}&\frac{\beta_1\beta_2\omega\epsilon K_z}{K_f}\,\mathrm{tg}\,\beta_1 h\,\mathrm{ctg}\,K_z(c-h)\,(q_1-q_2)\\&+Y_F^2\omega\mu_o K_z K_f\,\mathrm{ctg}\,\beta_2 h tg K_z(c-h)\,(r_1-r_2)\\&+Y_F\beta_1\,\mathrm{tg}\,\beta_1 h\,\mathrm{ctg}\,\beta_2 h(q_1K_z^2-\omega^2\epsilon\mu_o r_2)\\&+Y_F\beta_2(\omega^2\epsilon\mu_o r_1-K_z^2 q_2)=0\end{aligned}$$

in which the radial propagation constant K_c is implicitly formulated in K_z and β_i $(i = 1, 2)$. Hence, K_c can be obtained by solving this nonlinear equation that is independent of transverse coordinates φ and r. Results indicate that there is a finite number of modes (volume modes) for $K_c^2 > 0$ and an infinite number of modes (surface modes) for $K_c^2 < 0$. In our formulation, only the lowest volume V modes are obtained if the infinite summation is truncated into a finite one. On the other hand, the propagation constants β_1 and β_2 in the ferrite, as well as K_z in the dielectric, can be simply calculated from each value of K_c. Now, the constants A_{2n}, B_{1n}, and B_{2n} are expressed in terms of A_{1n}, such as

$$\begin{aligned}A_{2n}&=M_{A2}(h)A_{1n}\\B_{1n}&=M_{B1}(h)A_{1n}\\B_{2n}&=M_{B2}(h)A_{1n}\end{aligned}\tag{9}$$

where

$$\begin{aligned}M_{A2}(h)&=\frac{H_1G_{32}-H_3G_{12}}{\Delta}\\M_{B1}(h)&=\frac{G_{11}H_3-G_{31}H_1}{\Delta}\\\Delta&=G_{11}G_{32}-G_{12}G_{31}\end{aligned}$$

and

$$\begin{aligned}M_{B2}(h)=\frac{1}{G_{23}\Delta}\,[&G_{12}(G_{21}H_3-G_{31}H_2)\\&+G_{32}(G_{11}H_2-G_{21}H_1)]\end{aligned}$$

with the following elements:

$$\begin{aligned}G_{11}&=\frac{K_c}{\omega\mu_0}P_2\cos\beta_2 h\\G_{12}&=-\frac{\omega\varepsilon}{K_c}\cos K_z(c-h)\\G_{31}&=\frac{K_c}{K_f}P_2\cos\beta_2 h\\G_{21}&=\frac{K_c}{\omega\mu_0}r_2\cos\beta_2 h\\G_{23}&=\frac{K_z}{K_c}\cos K_z(c-h)\\G_{32}&=\frac{K_z}{K_c}\sin K_z(c-h)\\H_1&=\frac{K_c}{\omega\mu_0}P_1\cos\beta_1 h\\H_2&=-\frac{K_c}{\omega\mu_0}r_1\cos\beta_1(h)\\H_3&=-\frac{K_c}{K_f^2}P_1\sin\beta_1(h).\end{aligned}$$

2) Field Matching of Two Adjacent Annuli: This field matching is to derive complex amplitudes of the fields in the last annulus in terms of its first counterpart. This is simply done by the use of continuity conditions of the tangential-field components at the interface of two adjacent annuli gradually from outer to inner in sequential order. With these conditions, four equations are obtained over the cylindrical surface $r = R_{T+1}$ between Tth and $(T + 1)$th annuli (see the Appendix for details). Thus, the complex field amplitudes defined in the last annulus waveguide are characterized by those of its first counterpart as follows:

$$[A_{\mathrm{inlv}}^J]=[C_1]\cdots[C_f][A_{\mathrm{inlv}}^1].\tag{10}$$

3) Field Matching of the Last Ferrite Annulus and Outer Air Region: Applying the continuity condition of the tangential field components at the interface $r = R_J$ between the outermost concentrically cylindrical ferrite loaded waveguide and the air region leads to the following equations:

$$\begin{aligned}E_z^J(R_J)&=E_z^{\mathrm{air}}(R_J)\\H_\varphi^J(R_J)&=H_\varphi^{\mathrm{air}}(R_J)\end{aligned}\tag{11a}$$

$$\begin{aligned}E_\varphi^J(R_J)&=E_\varphi^{\mathrm{air}}(R_J)\\H_z^J(R_J)&=H_z^{\mathrm{air}}(R_J).\end{aligned}\tag{11b}$$

Since these boundary conditions are applicable in the range of φ from0π to 2π, the n-related summation implicitly involved in (11) can be eliminated due to the orthgonality of the

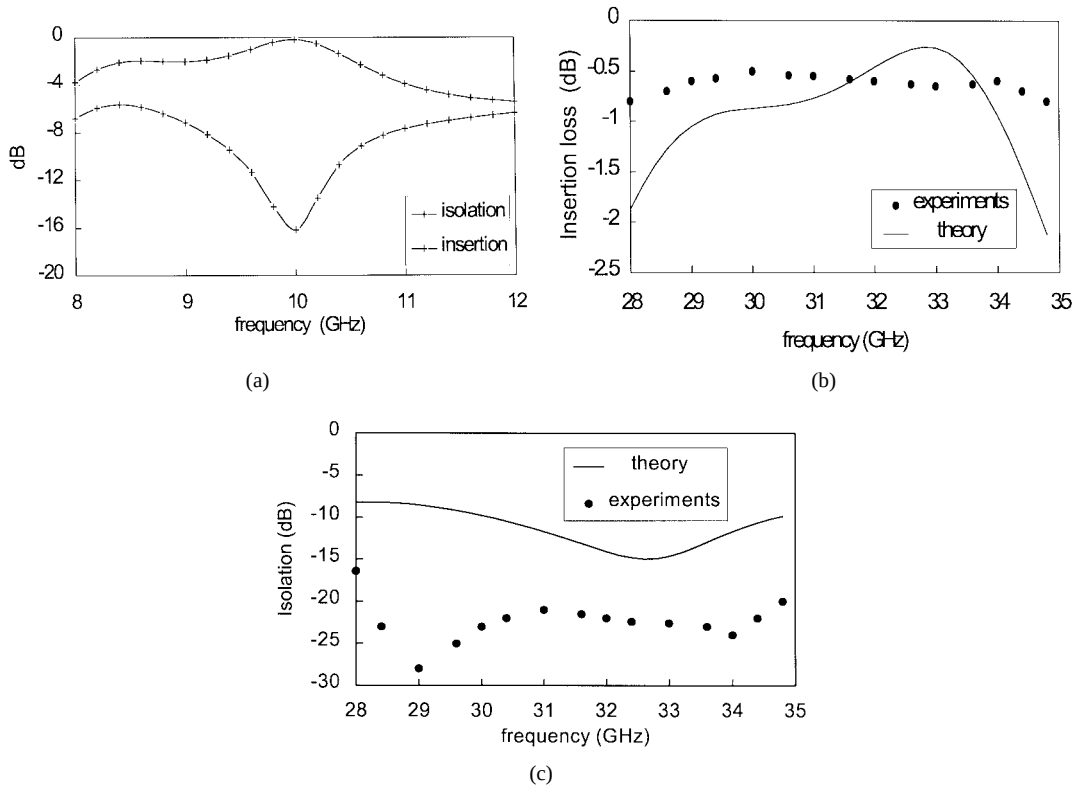

Fig. 3. Validation and comparison of our field theoretical model and its results against other available results. (a) Electrical characteristic of an X-band H-plane Y-junction circulator with a full-height ferrite post $R_0 = 3.5$ cm, (TT1-109), — our results, $+++$ [3]. (b) Results of a Ka-band wide-band H-plane Y-junction circulator with partial-height ferrite post for insertion loss: $\epsilon_d = 2.08$, $\epsilon_f = 15.0$, $R_0/h = 1.57$, $h = 0.78$ mm, $l = 4.16$ mm, $c = 0.978$ mm, $4\pi M_s = 5000$ G, $H_i = 200$ Oe, — our model, • • • experimental results [16]. (c) Results of a Ka-band wide-band H-plane Y-junction circulator with partial-height ferrite post for isolation: [the same parameters as above (b)] — our model, • • • experimental results [16].

exponential functions. Multiplying (11a) by $\cos\beta_m z$, and (11b) by $\sin\beta_m z$, and then integrating them from $z = 0$ to $z = c$ yield

$$\begin{aligned} &C_{1\mathrm{n}0}J_n(K_0R_f) + C_{2\mathrm{n}0}Y_n(K_oR_J) \\ &\quad = \frac{1}{c}\sum_{i=1}^{2}\sum_{l=1}^{2}\sum_{v=1}^{V} J_{nl}(K_{cv}R_J) \\ &\qquad \cdot [A^J_{\mathrm{inlv}}I1_{cimv}(h_J) + B^J_{\mathrm{inlv}}I2_{cimv}(h_J)] \\ &C_{1\mathrm{n}0}J'_n(K_0R_J) + C_{2\mathrm{n}0}Y'_n(K_oR_J) \\ &\quad = \frac{1}{cY_0}\sum_{i=1}^{2}\sum_{l=1}^{2}\sum_{v=1}^{V} A^J_{\mathrm{inlv}}\Pi_{3\mathrm{inlv}}(R_J)I1_{cimv}(h_J) \\ &\qquad + [B^J_{1\mathrm{nlv}}\Pi_{33\mathrm{nlv}}(R_J) + B^J_{2\mathrm{nlv}}\Pi_{34nv}(R_J)]I2_{cimv}(h_J) \end{aligned} \tag{12}$$

for $m = 0$ and (13), shown at the bottom of the following page, for $m \geq 1$, and $\beta_m = (m\pi/c)$, $m = 1, 2, \cdots, M$.

Based on the above six inhomogeneous equations, the complex amplitudes $C_{1\mathrm{n}0}$, $C_{2\mathrm{n}0}$, $C_{1\mathrm{nm}}$, $C_{2\mathrm{nm}}$, $D_{1\mathrm{nm}}$, $D_{2\mathrm{nm}}$ are given in terms of A^J_{inlv}, $B^J_{1\mathrm{nlv}}$, and $B^J_{2\mathrm{nlv}}$. Moreover, they can also be formulated in terms of A^1_{inlv} while (9) and (10) are applied. Once this field-matching process has been accomplished, the fields must be matched between the three rectangular waveguides and Y-junction region at the natural boundary of the Y-junction. However, we will not discuss this here for the sake of brevity, and interested readers may refer to [3], [4], [15], and [16] for details.

III. Results and Discussion

The equations derived in the above section are now solved for characterizing the ferrite–sphere-based Y-junction circulator. The choice of a finite number of matching points leads to a finite number of coupled (simultaneous) inhomogeneous equations, and the infinite expanded series involved in the equations representing waveguide and cylindrical modes also have to be truncated for numerical calculations. These two requirements should guarantee the result accuracy within the following criteria: the output power coming out of the three ports, i.e., the reflected power from the input port and the output power from the other two ports, should equal the incident power. This can be easily examined in the analysis. A rapid convergence of the finite expanded series should be observed. This can be done by first selecting a specific number of the matching points and then obtaining certain mode amplitudes, and then increasing the matching point number and observing the difference between the two consecutive calculations of the mode amplitudes. If the difference is negligible, the matching points are considered sufficient.

To begin with, an H-plane Y-junction having the full/partial-height ferrite post are modeled to validate our

analysis technique. Fig. 3(a) shows our frequency-dependent results compared to the X-band theoretical results reported in [3] for the full-height case, indicating an excellent agreement. Fig. 3(b) and (c) give our theoretical results compared with Ka-band experimental results reported in [16] for a partial-height case. It can be found that our theoretical results of insertion loss agree well with the experiments, although the difference is large for the isolation curve. This may be caused by simplified field expressions [12], [15] adopted in our eigenmode expansion, as well as the metal step action in the Y-junction. For small κ/μ, the simplified analysis is effective, but the error should not be neglected for the case of a large value in Ka-band. A ferrite post with operating frequencies lower than 50 GHz usually requires a saturated magnetization to achieve a larger bandwidth. Nevertheless, a wanted magnetization for saturation at 90 GHz may exceed 10 000, leading to unrealistic situation with the state-of-the art materials. Therefore, our simplified expression in connection with the eigenmode expansion should be effective to generate accurate results. To understand the circulating mechanism better, the calculation of a power-density flow in the radial direction of the Y-junction is desirable, which is defined simply by $\vec{P}_r = \frac{1}{2}\,\mathrm{Re}(\vec{E}\times\vec{H}^*)\cdot\vec{n}$ where $\vec{n}$ is the unit vector in the radial direction. Fig. 4(a) and (b) plots the power-density flow as a function of φ in full-height ferrite-post and air regions, respectively. Fig. 4(b) denotes that as r/R approaches 1 in the isolated port ($\varphi = 240° - 360°$), $\vec{P}_r$ is approximately zero. The signal power injected into the input port ($\varphi = 120° - 240°$) is almost completely transmitted into the output port ($\varphi = 0° - 120°$), thereby achieving the circulating function. In addition, the power density flowing into the input port is positive, while it remains negative at the output port. This is normal in relation to the signal-flow orientation. The input and output power-density flow in a closed cycle at any radius (air or ferrite region) is always balanced and conserved. This fact can be expected, as the ferrite is considered lossless in our analysis and no power is dissipated inside the Y-junction area.

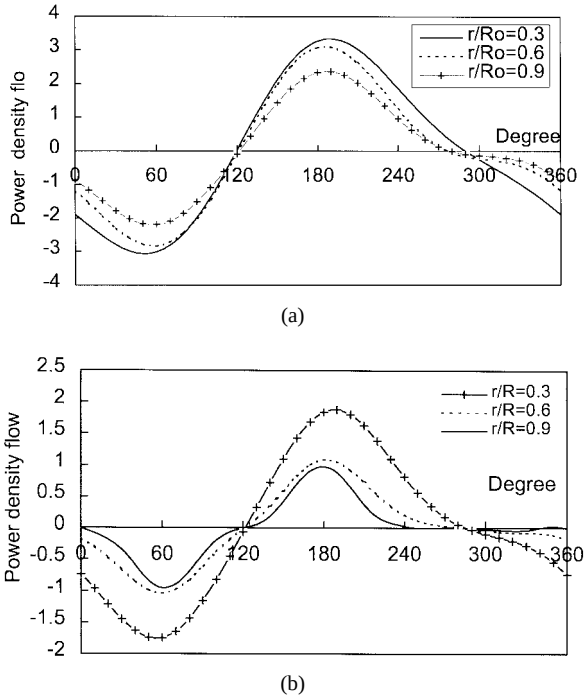

(a)

(b)

Fig. 4. Normalized radial power-density flow profile in the $z = 0$ plane for the X-band H-plane Y-junction circulator with a full-height sample (TT1-109): $R = a/\sqrt{3}$, $R_0 = 3.5$ cm, and $f_0 = 10$ GHz, The input port at 180°). (a) Inside of the ferrite post $(0 < r < R_0)$. (b) Outside of the ferrite post $(R_0 < r < R)$.

Following the validity of our analysis technique with the above two structures (full- and partial-height ferrite posts), our attention now focuses on the modeling and analysis of a class of three-dimensional ferrite–sphere-based waveguide circulators operating at millimeter-wave frequencies. Fig. 5(a)

$$
\begin{aligned}
&C_{1\mathrm{nm}}I_n(K_aR_J) + C_{2\mathrm{nm}}K_n(K_aR_J)\\
&\quad = \frac{2}{c}\sum_{i=1}^{2}\sum_{v=1}^{2}\sum_{l=1}^{V} J_{nl}(K_{cv}R_J)[A^J_{\mathrm{inlv}}I1_{cimv}(h_J) + B^J_{\mathrm{inlv}}I2_{cimv}(h_J)]\\
&D_{1\mathrm{nm}}I_n(K_aR_J) + D_{2\mathrm{nm}}K_n(K_aR_J)\\
&\quad = \frac{2}{c}\sum_{i=1}^{2}\sum_{v=1}^{2}\sum_{l=1}^{V} J_{nl}(K_{cv}R_J)[A^J_{\mathrm{inlv}}\frac{\beta_{iv}}{\omega\mu_0}t_{iv}I1_{simv}(h_J) + B^J_{1\mathrm{nlv}}I2_{\mathrm{sivm}}(h_J)]\\
&\frac{jm\pi}{K_a^2c}\ \frac{n}{R_J}[C_{1nm}I_n(K_aR_j) + C_{2nm}K_n(K_aR_j)] + \frac{\omega\mu_0}{K_a}[D_{1nm}I'_n(K_aR_j)D_{2nm}K'_n(K_aR_J)]\\
&\quad = \frac{-2}{c}\sum_{i=1}^{2}\sum_{\nu=1}^{2}\sum_{l=1}^{V} A^J_{\mathrm{inlv}}\Pi_{4\mathrm{inlv}}(R_J)I1_{\mathrm{sivm}}(h_J) + j[B^J_{1\mathrm{nlv}}\Pi_{43\mathrm{nlv}}(R_J) + B^J_{2\mathrm{nlv}}\Pi_{44\mathrm{nlv}}(R_J)]I2_{\mathrm{sivm}}(h_J)\\
&\frac{\omega\varepsilon_0}{k_a}[C_{1\mathrm{nm}}I'_n(k_aR_J) + C_{2\mathrm{nm}}K'_n(k_aR_J)] + \frac{m\pi}{K_a^2c}\ \frac{n}{R_J}[D_{1\mathrm{nm}}I_n(k_aR_J) + D_{2\mathrm{nm}}K_n(k_aR_J)]\\
&\quad = \frac{2}{c}\sum_{i=1}^{2}\sum_{l=1}^{2}\sum_{v=1}^{V}\{A^J_{\mathrm{inlv}}\Pi_{3\mathrm{inlv}}(R_J)I1_{\mathrm{civm}}(h_J) + [B^J_{1\mathrm{nlv}}\Pi_{33\mathrm{nlv}}(R_J) + B^J_{2\mathrm{nlv}}\Pi_{34\mathrm{nlv}}(R_J)]I2_{\mathrm{civm}}(h_J)\}
\end{aligned}
\tag{13}
$$

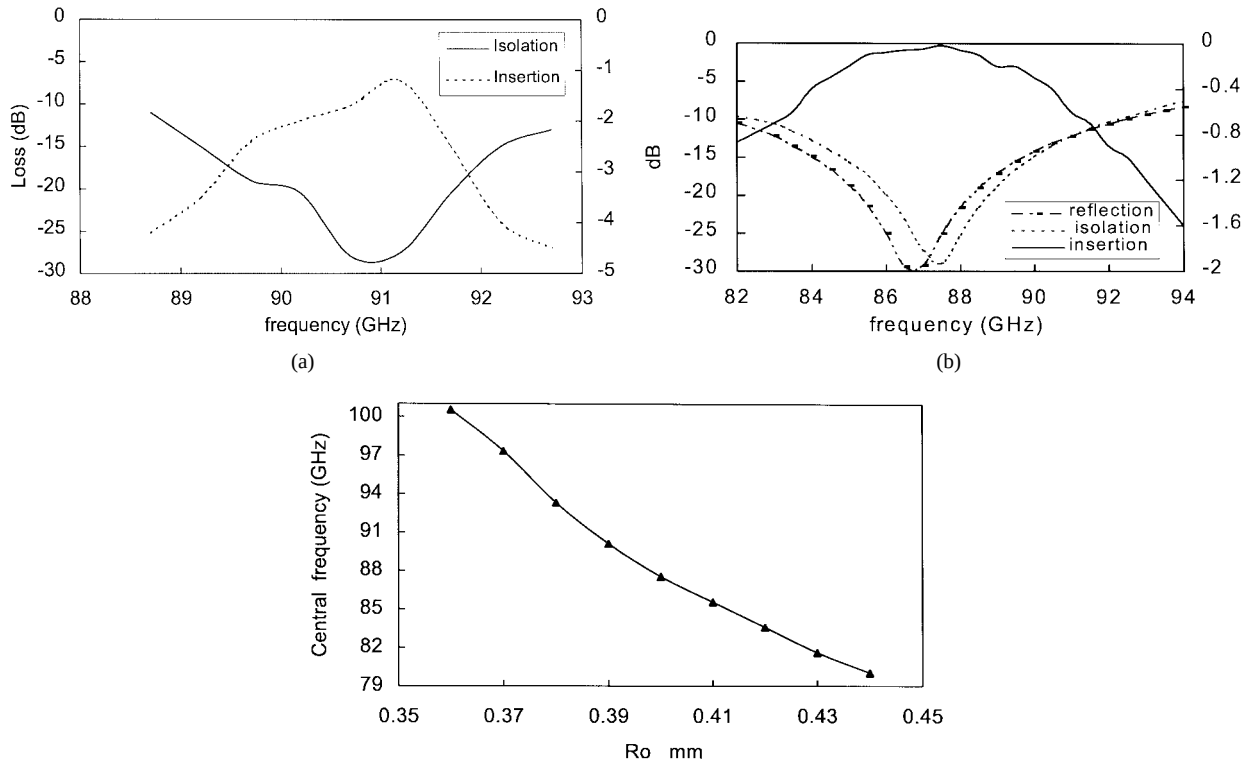

Fig. 5. Electrical characteristic of a W-wave band H-plane Y-junction circulator with a compound crystal Ni–Zn ferrite sphere: waveguide dimension $a \times b = 2.54 \times 1.27$ mm^2, sphere radius $R_0 = 0.4$ mm $\pm 5\%$, $c = 0.635$ mm, $\epsilon_d = 2.25$, $\epsilon_f = 13.5$, $R = a/\sqrt{3}$, permanent magnets $H_e > 1700$ Oe, $4\pi M_s = 5000$ G, ΔH (loss) < 120 Oe. (a) Measured results. (b) Calculated results. (c) Central operating frequency versus the sphere radius R_0.

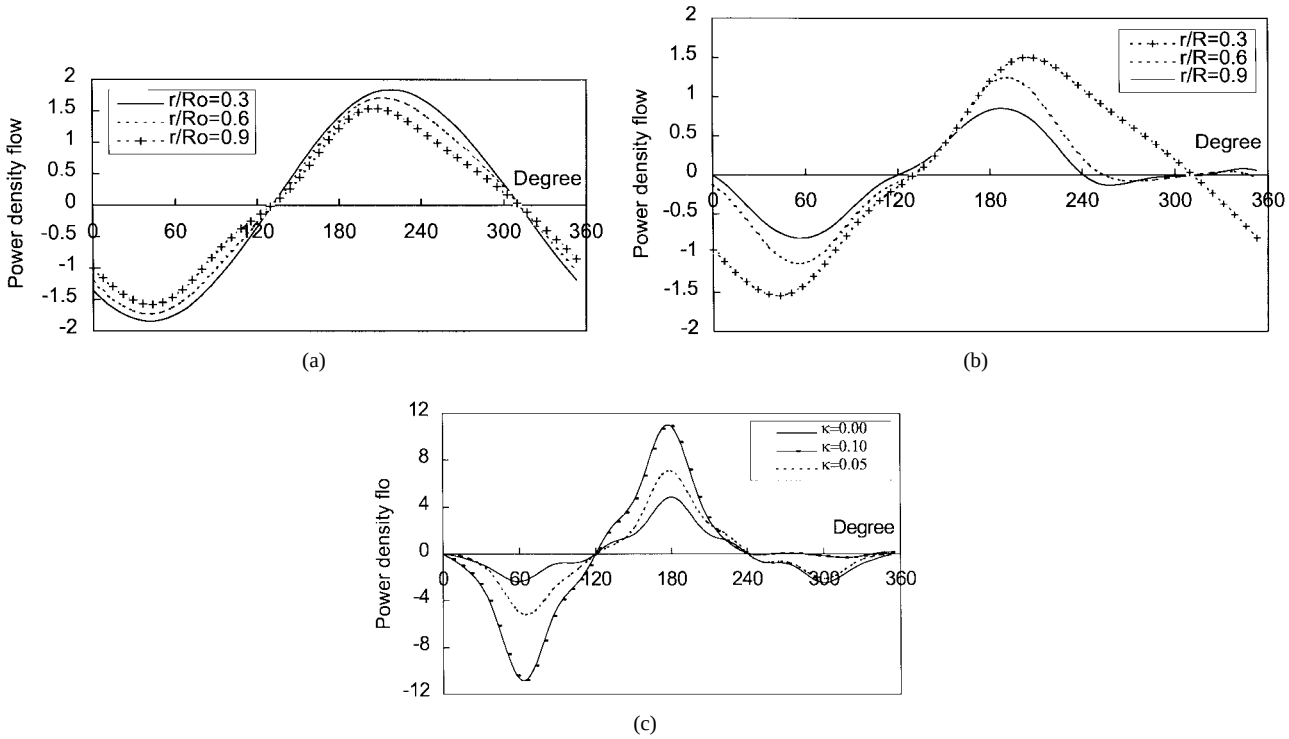

Fig. 6. Normalized radial power-density flow profile in the $z = 0$ plane of a ferrite–sphere-based WR-10 waveguide H-plane Y-junction: $a \times b = 2.54 \times 1.27$ mm^2, sphere radius $R_0 = 0.4$ mm $\pm 5\%$, $c = 0.635$ mm, $\epsilon_d = 2.25$, $\epsilon_f = 13.5$, $f_0 = 90$ GHz, permanent magnets $H_e > 1700$ Oe, $4\pi M_s = 5000$ G, ΔH (loss) < 120 Oe. (The input port at 180°). (a) Inside of the ferrite sphere for different radius $(0 < r < R_0)$. (b) Outside of the ferrite sphere for different radius $(R_0 < r < R)$. (c) At the position of $r = 0.9R$ for an off-diagonal element (of permeability tensor cases).

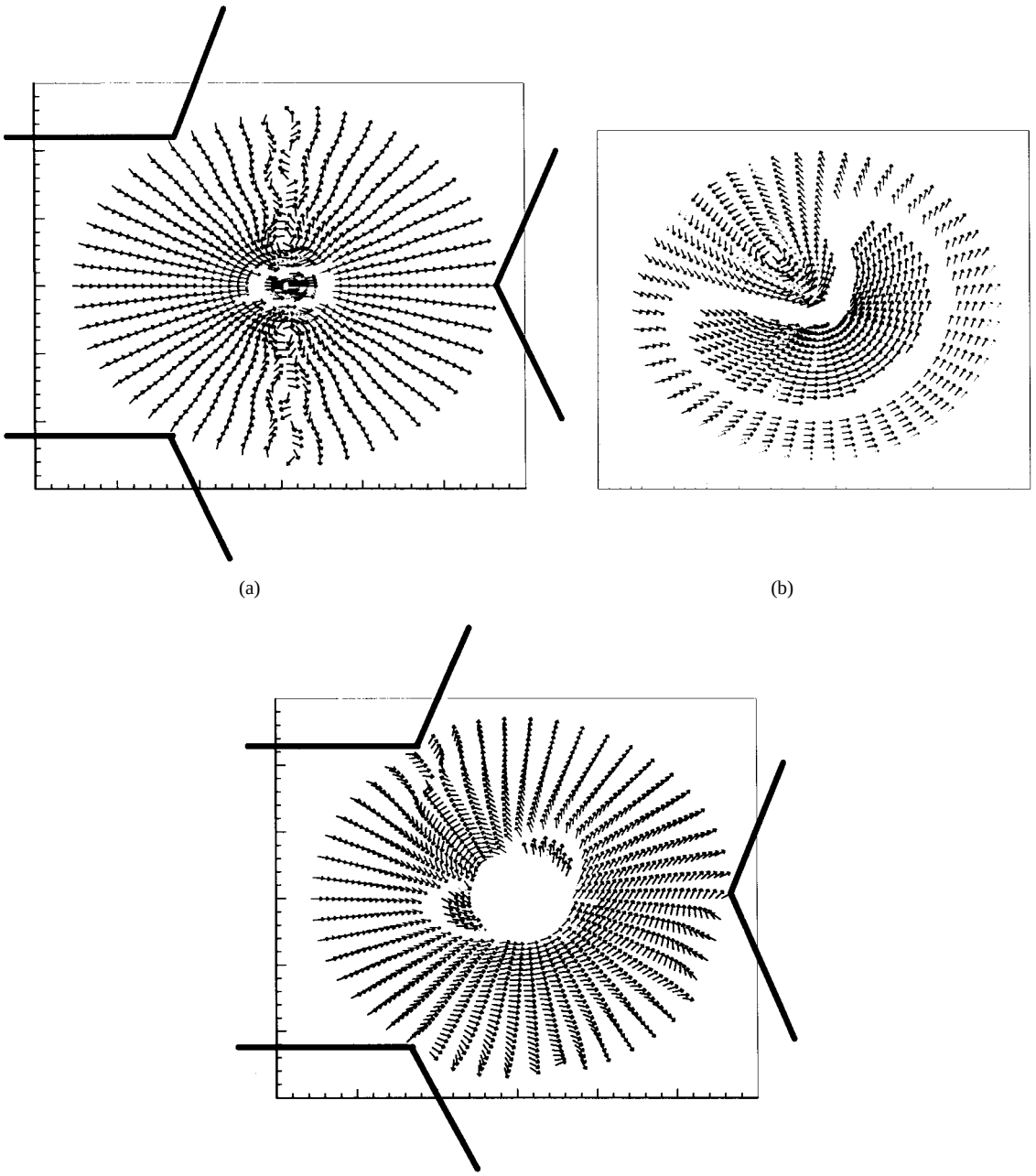

Fig. 7. Complete picture of power-density flow profile in the $z = 0$ plane of an X-band full-height ferrite post waveguide H-plane Y-junction circulator: $a \times b = 2.286 \times 1.143$ cm^2, post radius $R_0 = 3.5$ cm, $R = a/\sqrt{3}$, $f_0 = 10$ GHz, (the input port at 180°, the output at 60°, the isolated port at 300°). (a) Demagnetized case if $\kappa = 0.0 (0 < r < R)$. (b) $\kappa = 0.37$, inside of the ferrite post $(r < R_0)$. (c) $\kappa = 0.37$, outside of the ferrite post $(R_0 < r < R)$.

and (b) shows measured and calculated electrical characteristics of new circulators versus frequency in terms of the insertion and reflection loss, as well as isolation for W-band applications. The insertion loss obtained by our analysis is better than our experimental results, which can be attributed to the absence of a loss factor in the modeling. It is also observed that the reflection and isolation are better than 28 dB for W-band. However, the two frequency-response curves are shifted from each other, indicating that a prescribed electrical performance may be preferred as to which factor is emphasized in the design. This also gives rise to a fundamental question as to whether it is possible to achieve the optimized characteristics for all the targeted parameters. It is found that the calculated center frequencies are 3.81% lower than their measured counterparts, considering the difference between Fig. 5(a) and (b). This frequency shift is attributed to the prescribed $\pm 5\%$ fabrication tolerance of our ferrite–sphere radius designed for our experiment, and Fig. 5(c) displays the dependency of a center operating frequency with the sphere radius in the case that a bias external magnetic field is set to be 200 Oe. Although the center frequency of our proposed circulator is found to be sensitive to the ferrite–sphere radius,

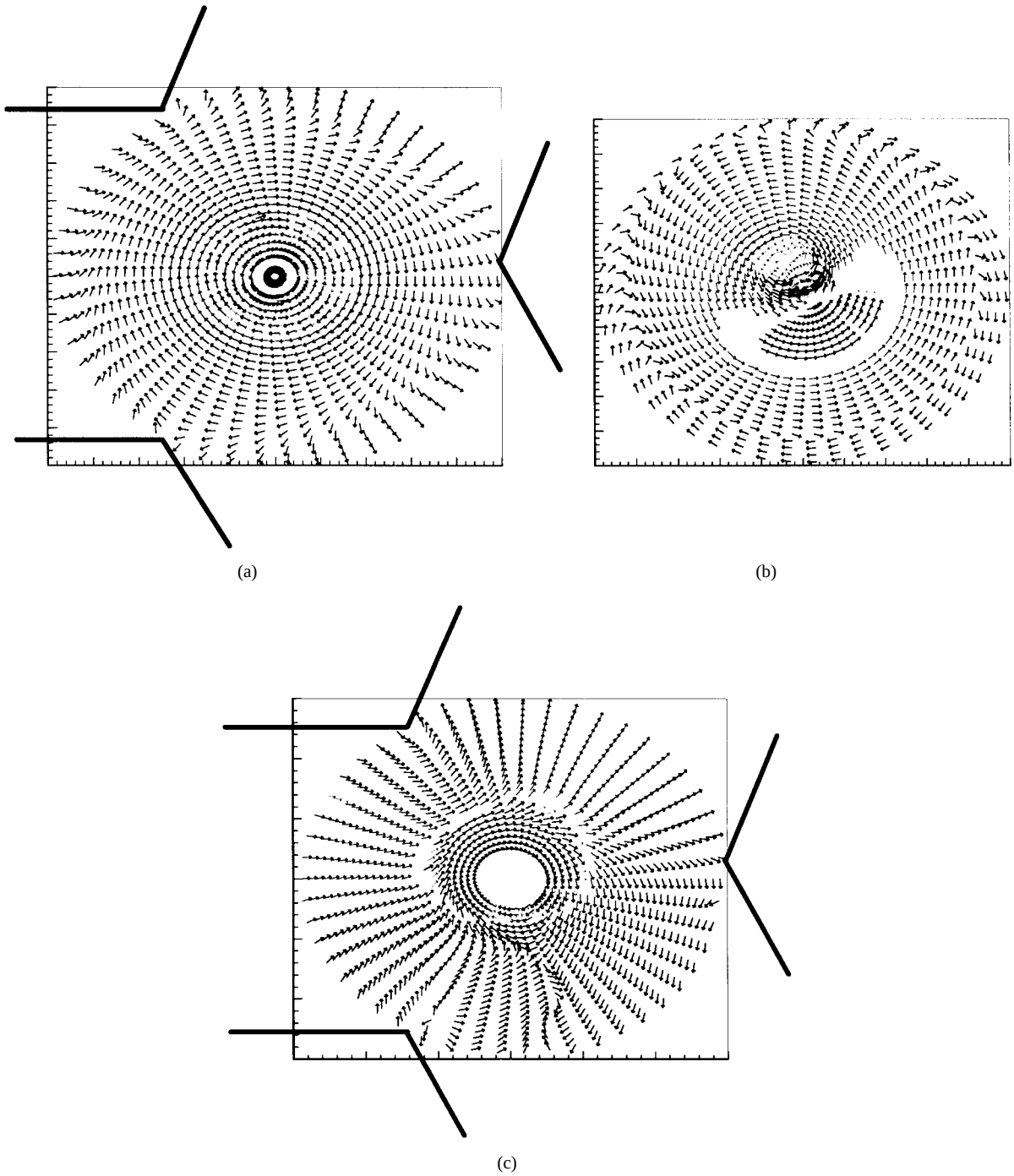

Fig. 8. Complete picture of power-density flow profile in the $z = 0$ plane of a W-band ferrite–sphere waveguide H-plane Y-junction circulator: $a \times b = 2.54 \times 1.27$ mm^2, sphere radius $R_0 = 0.4$ mm, $R = a/\sqrt{3}$, $f_0 = 90$ GHz, (the input port at 180°, the output at 60°, the isolated port at 300°). (a) Demagnetized case if $\kappa = 0.0$ $(0 < r < R)$. (b) $\kappa = 0.37$, inside of the ferrite sphere $(R_0 < r < R)$. (c) $\kappa = 0.37$, outside of the ferrite sphere $(r > R_0)$.

a large-scale batch fabrication of small ferrite sphere with nearly identical radius can be easily obtained to meet the demand at a given frequency. Fig. 6(a)–(c) gives calculated profiles of the power-density flow $\overrightarrow{P}_r$ in both the ferrite and air regions as a function of the orientation angle φ for different radius defined in the first two figures and for different off-diagonal element κ of the permeability tensor. Similar to the two-dimensional case, the input and output power flows are kept well balanced. Interestingly, the maximum (or minimum) points of the positive and negative power-density curves, unlike the case of the full-height ferrite post circulator, are shifted away from the input and output directions, as indicated in Fig. 6(a) and (b) for different radius. As the radius begins its decreasing from $a/\sqrt{3}$ to zero, the maximum positive positions move from 180° counterclockwise, while the maximum negative positions move from 60° clockwise. This is quite different from the stationary behavior of the two-dimensional case. This phenomenon suggests that the ferrite

sphere operates in a different manner from the full height in circulating the signal waves. On the other hand, an adequate choice of an off-diagonal element, as shown in Fig. 6(c), is also important for the circulator operation that can readily optimized.

To better illustrate the circulating mechanism of the proposed ferrite sphere, a complete picture of the power-density flow vector profile in the $z = 0$ plane of the Y-junction is given in Fig. 8(a) for $\kappa = 0.0$ and Fig. 8(b) and (c) for $\kappa = 0.1$. To facilitate our discussion, the similar plots are also shown in Fig. 7(a)–(c) for the full-height ferrite post. It is well known that a full-height ferrite-post loaded Y-junction is resonant with the TM_{110} mode, which is easily excited by the TE_{10} mode of the rectangular waveguide. Such a TM_{110} mode presents a field pattern that can be generated by the sum of a pair of similar contrarotating modes, and the RF magnetic field inside the ferrite at the center of the cavity is circularly polarized for each side (right- or left-hand side) of rotation. With the demagnetized ferrite, both contrarotating modes become resonant at the same frequency and the output ports will guide two signal waves of about equal magnitude, as shown in Fig. 7(a). If the standing-wave pattern is rotated through 30° as the ferrite post is suitably magnetized, one output port is then situated at a voltage null of the $\mathrm{TM}_{\pm 110}$ modes, and the fields at the other two ports are equal in magnitude, as shown in Fig. 7(b) and (c). To some extent, the device behaves like a transmission cavity between the input port and one output port, while the other port is isolated.

However, the ferrite–sphere-junction circulator operates in a turnstile fashion, and its rotating modes propagate along the ferrite–sphere axis coinciding with the direction of an applied external magnetic field H_0. The degenerate frequencies of the counter-rotating modes are approximately equal to the resonant frequencies of the ferrite sphere as if the latter were treated as a dielectric resonator and the field is distributed symmetrically over the input port. In the ferrite–sphere-junction circulator, the lowest degenerate mode is TE_{111} although the real lowest mode of operation in a dielectric sphere is TE_{101} that, nevertheless, does not have the function of a φ-dependent field for circulating electromagnetic wave. Magnetizing the ferrite sphere increases the propagation constant of one rotating mode and decreases the other so that the resonant frequencies of such degenerate rotating modes are split off like the partial-height ferrite post in Y-junction circulator since these modes are circularly polarized in opposite orientations, experiencing different permeability. As a result, the field profiles of the degenerate rotating modes turn with an angle along the φ direction in opposite orientations. Through adjusting the applied external magnetic field and adequately selecting the radius of the ferrite sphere at a given frequency, the fields of the two split resonant modes may be null in the isolated port, while adding up at the output port. The power injected from the input port could completely be circulated into the output port if the ports are well matched. It is observed from Fig. 8(b) and (c) that the ferrite–sphere circulator is not based on the transmission cavity model, but a resonant cavity model. The input power is not directly related to the output, but turned a circle around the ferrite sphere toward the output port.

IV. Conclusions

A new way of designing H-plane waveguide Y-junction circulator is proposed in this paper. Instead of the conventional form of a ferrite post such as the cylinder ferrite post of full height, a ferrite–sphere topology is used in the circulator design for potentially low-cost millimeter-wave applications. The proposed scheme presents advantageous features: namely, easy-to-fabricate with the well-matured micromachining technique, and east-to-assemble in view of the waveguide mounting. Considering the fact that the proposed structure is three-dimensional in nature as compared with the two-dimensional full-height post, the development of an efficient and accurate modeling technique is a challenging issue. In addition, the self-inconsistent three coordinates are simultaneously involved in the analysis. To solve this troublesome problem, a modal field-matching technique is developed to calculate field profiles of the structure as well as to characterize the proposed circulator. This technique is based on a segmentation of the spherical geometry so that the mode-matching procedure can be effectively made in the mixed cylindrical and rectangular coordinates. Results are obtained and compared very well with available experiments for a full-height circulator to validate the modeling strategy.

A comprehensive comparable study between the new and conventional circulators is made to show that the electrical behaviors of the new structure are distinct and radial power-density profiles are not stationary, as in the case of the full-height ferrite post circulator for different geometrical parameters. It is also found that the circulating mechanism of the ferrite–sphere post is different from its full-height ferrite counterpart in that the new structure operates in a turnstile fashion with the nature of resonance. While the operating mechanism of the conventional device can be well explained by a transmission cavity model. Our calculated and measured results are also presented for W-band circulators with the proposed ferrite–sphere technique, indicating some interesting characteristics such as the frequency-offset behavior of the isolation and reflection curves. In addition, radial power-density profiles are plotted inside and outside the ferrite sphere to illustrate its intrinsic circulating mechanism, as well as its difference as compared to its full-height ferrite structure. It is suggested that an excellent circulating performance with the proposed ferrite sphere be achieved by adjusting the externally applied magnetic field and adequately selecting the radius of the ferrite sphere at a given frequency.

Our theoretical and experimental results as well as discussion on parametric effects indicate that a field-theoretical analysis is necessary for an accurate design of such a new circulator, and also that ferrite–sphere scheme is an efficient alternative in the design of a quality circulator for millimeter-wave applications.

Appendix

The tangential fields $(E_t,\ H_t)$ are formulated for mode matching as follows:

$$E_z^T(R_{T+1}) = E_z^{T+1}(R_{T+1})$$
$$H_\varphi^T(R_{T+1}) = H_\varphi^{T+1}(R_{T+1}) \qquad \text{(A-1)}$$

$$H_z^T(R_{T+1}) = H_z^{T+1}(R_{T+1})$$
$$E_\varphi^T(R_{T+1}) = E_\varphi^{T+1}(R_{T+1}) \tag{A-2}$$

where

$$E_z^T(R_{T+1}) = \begin{cases} E_{zF}^T(R_{T+1}), & 0 \le z < h_T \\ E_{zD}^T(R_{T+1}), & h_T \le z < C \end{cases}$$
$$E_\varphi^T(R_{T+1}) = \begin{cases} E_{\varphi F}^T(R_{T+1}), & 0 \le z < h_T \\ E_{\varphi D}^T(R_{T+1}), & h_T \le z \le C \end{cases}$$
$$H_z^T(R_{T+1}) = \begin{cases} H_{zF}^T(R_{T+1}), & 0 \le z < h_T \\ E_{zD}^T(R_{T+1}), & h_T \le z < C \end{cases}$$
$$H_\varphi^T(R_{T+1}) = \begin{cases} H_{\varphi F}^T(R_{T+1}), & 0 \le z < h_T \\ H_{\varphi D}^T(R_{T+1}), & h_T \le z \le C \end{cases}$$
$$E_z^{T+1}(R_{T+1}) = \begin{cases} E_{zF}^{T+1}(R_{T+1}), & 0 \le z < h_{T+1} \\ E_{zD}^{T+1}(R_{T+1}), & h_{T+1} \le z < C \end{cases}$$
$$E_\varphi^{T+1}(R_{T+1}) = \begin{cases} E_{\varphi F}^{T+1}(R_{T+1}), & 0 \le z < h_{T+1} \\ E_{\varphi D}^{T+1}(R_{T+1}), & h_{T+1} \le z < C \end{cases}$$
$$H_\varphi^{T+1}(R_{T+1}) = \begin{cases} H_{\varphi F}^{T+1}(R_{T+1}), & 0 \le z < h_{T+1} \\ H_{\varphi D}^{T+1}(R_{T+1}), & h_{T+1} \le z \le C \end{cases}$$
$$H_z^{T+1}(R_{T+1}) = \begin{cases} H_{zF}^{T+1}(R_{T+1}), & 0 \le z < h_{T+1} \\ E_{zD}^{T+1}(R_{T+1}), & h_{T+1} \le z \le C. \end{cases}$$

Since the continuity condition of the tangential-field components defined at interfaces is applicable to φ in the range of 0π–2π, the summation related to φ in the expressions of (6) and (7) can be effectively eliminated due to the orthogonal properties of exponential function. With the consideration of existence of the lowest volume modes, they are all added up in the following equations. Multiplying (A-1) by $\cos\beta_m z$ and (A-2) by $\sin\beta_m z$ and integrating them from $z=0$ to $z=c$ leads to (A-3)–(A-6), shown at the bottom of this page, where $\beta_m = (m\pi/c)$, $v, m = 1, 2, \cdots, V$ as follows:

$$\Pi_{3\mathrm{inlv}}(r) = Y_f \frac{K_{cv}}{K_f}\left[P_i R'_{nl}(K_{cv}r) - r_i \frac{nR_{nc}(K_{cv}r)}{K_{cv}r}\right], \quad i = 1,2$$
$$\Pi_{33\mathrm{nlv}}(r) = \frac{\omega\epsilon}{K_{cv}} R'_{nl}(K_{cv}r)$$
$$\Pi_{34\mathrm{nlv}}(r) = \frac{K_{zv}}{K_{cv}^2}\frac{n}{r} R_n(K_{cv}r)$$
$$\Pi_{4inlv}(r) = \frac{K_{cv}\beta_{iv}}{K_f^2}\left[q_i R'_{nl}(K_{cv}r) - P_i \frac{nR_{nl}(K_{cv}r)}{K_{cv}r}\right], \quad i = 1,2$$
$$\Pi_{43nlv}(r) = \frac{K_{zv}}{K_{cv}^2}\frac{n}{r} R_{nl}(K_{cv}r)$$
$$\Pi_{44\mathrm{nlv}}(r) = \frac{\omega\mu_0}{K_{cv}} R'_{nl}(K_{cv}r)$$
$$I1_{\mathrm{civm}}(z) = \int_0^z \cos\beta_{iv}z \cos\beta_m z\, dz$$
$$I2_{\mathrm{civm}}(z) = \int_z^c \cos K_{zv}(c-z)\cos\beta_m z\, dz$$
$$I1_{\mathrm{sivm}}(z) = \int_0^z \sin\beta_{iv}z \cdot \sin\beta_m z\, dz$$
$$I2_{\mathrm{sivm}}(z) = \int_z^c \sin K_{zv}(c-z)\sin\beta_m z\, dz.$$

If the related terms in (12) are substituted, the unknowns B_{inlv} in (A-3)–(A-6) are formulated in terms of A_{inlv} so that $4 \times V$

$$\sum_{i=1}^{2}\sum_{l=1}^{2}\sum_{v=1}^{V} J_{nl}(K_{cv}^{T+1}R_{T+1})\left\{A_{\mathrm{inlv}}^{T+1} I1_{\mathrm{civm}}(h_{T+1}) + B_{\mathrm{inlv}}^{T+1} I2_{\mathrm{civm}}(h_{T+1})\right\}$$
$$= \sum_{i=1}^{2}\sum_{l=1}^{2}\sum_{v=1}^{V} J_{nl}(K_{cv}^{T}R_{T+1})\left\{A_{\mathrm{inlv}}^{T} I1_{\mathrm{civm}}(h_{T}) + B_{\mathrm{inlv}}^{T} I2_{\mathrm{civm}}(h_{T})\right\} \tag{A-3}$$
$$\sum_{i=1}^{2}\sum_{l=1}^{2}\sum_{v=1}^{V} J_{nl}(K_{cv}^{T+1}R_{T+1})\left\{A_{\mathrm{inlv}}^{T+1} I1_{\mathrm{sivm}}(h_{T+1})\beta_{iv}^{T+1} + B_{\mathrm{inlv}}^{T+1} I2_{\mathrm{sivm}}(h_{T+1})\right\}$$
$$= \sum_{i=1}^{2}\sum_{l=1}^{2}\sum_{v=1}^{V} J_{nl}(K_{cv}^{T}R_{T+1})\left\{A_{\mathrm{inlv}}^{T} I1_{\mathrm{sivm}}(h_{T})\beta_{iv}^{T} + B_{\mathrm{inlv}}^{T} I2_{\mathrm{sivm}}(h_{T})\right\} \tag{A-4}$$
$$\sum_{i=1}^{2}\sum_{l=1}^{2}\sum_{v=1}^{V} \left\{A_{\mathrm{inlv}}^{T+1}\Pi_{3\mathrm{inlv}}^{T+1} I1_{\mathrm{civm}}(h_{T+1}) + (B_{1\mathrm{nlv}}^{T+1}\Pi_{33\mathrm{nlv}}^{T+1} + B_{2\mathrm{nlv}}^{T+1}\Pi_{34\mathrm{nlv}}^{T+1}(R_{T+1}))I2_{\mathrm{civm}}(h_{T+1})\right\}$$
$$= \sum_{i=1}^{2}\sum_{l=1}^{2}\sum_{v=1}^{V} \left\{A_{\mathrm{inlv}}^{T}\Pi_{3\mathrm{inlv}}^{T} I1_{simv}(h_T) + [B_{\mathrm{inlv}}^{T}\Pi_{34\mathrm{nlv}}^{T}(R_{T+1}) + B_{2nv}^{T}\Pi_{33\mathrm{nlv}}^{T}(R_{T+1})I2_{\mathrm{sivm}}(h_T))\right\} \tag{A-5}$$
$$\sum_{i=1}^{2}\sum_{l=1}^{2}\sum_{v=1}^{V} \left\{A_{\mathrm{inlv}}^{T+1}\Pi_{4inlv}^{T+1} I1_{\mathrm{sivm}}(h_{T+1}) + (B_{1\mathrm{nlv}}^{T+1}\Pi_{43nlv}^{T+1}(R_{T+1}) + B_{2\mathrm{nlv}}^{T+1}\Pi_{44\mathrm{nlv}}^{T+1}(R_{T+1}))I2_{\mathrm{sivm}}(h_{T+1})\right\}$$
$$= \sum_{i=1}^{2}\sum_{l=1}^{2}\sum_{v=1}^{V} \left\{A_{\mathrm{inlv}}^{T}\Pi_{4inlv}^{T} I1_{simv}(h_T) + (B_{1\mathrm{nlv}}^{T}\Pi_{44\mathrm{nlv}}^{T}(R_{T+1}) + B_{2\mathrm{nlv}}^{T}\Pi_{44\mathrm{nlv}}^{T}(R_{T+1}))I2_{\mathrm{sivm}}(h_T)\right\} \tag{A-6}$$

equations also contain $4 \times V$ unknowns A_{inlv}^{T+1}. By solving these equations, the complex amplitudes can be determined in terms of A_{inlv}^{T}. It can be written in a matrix form as follows:

$$[L]_{AV\times 4V} A_{\text{inlv}}^{T+1} = [R]_{4V\times 4V} A_{\text{inlv}}^{T} \quad \text{(A-7)}$$

$$\begin{aligned} A_{\text{inlv}}^{T+1} &= [L]_{4V\times 4V}^{-1} [R]_{4V\times 4V} A_{\text{inlv}}^{T} \\ &= [C_T]_{4V\times 4V} A_{\text{inlv}}^{T} \end{aligned} \quad \text{(A-8)}$$

in which $[L]$ and $[R]$ are left- and right-hand-side coefficient matrices of $4V \times 4V$, respectively. $[C_T]$ is also a $4V \times 4V$ matrix.

REFERENCES

[1] E. K. N. Yung *et al.*, "A novel waveguide Y-junction circulator with a ferrite sphere for millimeter waves," *IEEE Trans. Microwave Theory Tech.*, vol. 44, pp. 454–456, Mar. 1996.

[2] J. B. Castillo and L. E. Davis, "Computer aided design of 3-port waveguide junction circulators" *IEEE Trans. Microwave Theory Tech.*, vol. MTT-18, pp. 25–34, Jan. 1970.

[3] M. E. El-Shandwily *et al.*, "General field theory treatment of H-plane waveguide junction circulators," *IEEE Trans. Microwave Theory Tech.*, vol. MTT-21, pp. 392–403, June 1973.

[4] A. Khilla and I. Wolff, "Field theory treatment of H-plane waveguide junction with triangular ferrite post," *IEEE Trans. Microwave Theory Tech.*, vol. MTT-26, pp. 279–287, Apr. 1978.

[5] N. Okamoto, "Computer-aided design of H-plane waveguide junctions with full-height ferrites of arbitrary shape," *IEEE Trans. Microwave Theory Tech.*, vol. MTT-27, pp. 315–321, Apr. 1979.

[6] M. Koshiba and M. Suzuki, "Finite-element analysis of H-plane waveguide junction with arbitrary shaped ferrite post," *IEEE Trans. Microwave Theory Tech.*, vol. MTT-34, pp. 103–109, Jan. 1986.

[7] M. E. El-Shandwily *et al.*, "General field theory treatment of E-plane waveguide junction circulators N—Part I: Full-height ferrite configuration," *IEEE Trans. Microwave Theory Tech.*, vol. MTT-25, pp. 784–793, Sept. 1977.

[8] B. Owen, "The identification of modal resonances in ferrite loaded waveguide Y-junction and their adjustment for circulation," *Bell Syst. Tech. J.*, vol. 51, no. 3, pp. 595–627, 1972.

[9] J. Helszajn *et al.*, "Design data for radial waveguide circulators using partial height ferrite resonators," *IEEE Trans. Microwave Theory Tech.*, vol. MTT-23, pp. 288–298, Mar. 1975.

[10] J. Helszajn *et al.*, "Resonant frequencies, Q-factor, and susceptance slope parameter of waveguide circulators using weakly magnetized open resonators," *IEEE Trans. Microwave Theory Tech.*, vol. MTT-31. pp. 434–441, June 1983.

[11] ——, "Design of waveguide circulators with Chebyshev characteristics using partial height ferrite resonators," *IEEE Trans. Microwave Theory Tech.*, vol. MTT-32, pp. 908–917, Aug. 1984.

[12] W. Hauth, "Analysis Of circular waveguide cavities with partial height ferrite insert," in *Proc. European Microwave Conf.*, 1981, pp. 383–388.

[13] M. E. El-Shandwily *et al.*, "General field theory treatment of E-plane waveguide junction circulators N—Part II: Two disk ferrite configurations," *IEEE Trans. Microwave Theory Tech.*, vol. MTT-25, pp. 794–803, Sept. 1977.

[14] Y. Akaiwa, " A numerical analysis of waveguide H-plane Y junction circulators with circular partial height ferrite post," *Trans. IECE*, vol. E61, no. 8, pp. 609–617, Aug. 1978.

[15] W. B. Dou and S. F. Li, "On volume modes and surface modes in partial height ferrite circulators and their bandwidth expansion at millimeter wave band," *Microwave Opt. Technol. Lett.*, vol. 1, no. 6, pp. 200–208, Aug. 1988.

[16] W. B. Don and Z. L. Sun, "Millimeter wave ferrite circulators and rotators," *Int. J. Infrared Millimeter Waves*, vol. 17, no. 12, pp. 2034–2131, Dec. 1996.

[17] Y. Y. Tsai and A. S. Omar, "Field theoretical treatment of E-plane waveguide junctions with anisotropic medium," *IEEE Trans. Microwave Theory Tech.*, vol. 40, pp. 2164–2171, Dec. 1992.

[18] ——, "Field theoretical treatment of H-plane waveguide junctions with anisotropic medium," *IEEE Trans. Microwave Theory Tech.*, vol. 41, pp. 274–281, Feb. 1993.

[19] W. K. Hui and I. Wolff, "A multicomposite, multilayered cylindrical dielectric resonator for application in MMIC," *IEEE Trans. Microwave Theory Tech.*, vol. 42, pp. 415–423, Mar. 1994.

[20] C. M. Krowne and R. E. Neidert, "Theory and numerical calculation for radially inhomogeneous circuit ferrite circulators," *IEEE Trans. Microwave Theory Tech.*, vol. 44, pp. 419–431, Mar. 1996.

Edward Kai-Ning Yung (M'85–SM'85) was born in Hong Kong. He received the B.Sc., M.Sc., and Ph.D. degrees in electrical engineering from the University of Mississippi, Mississippi State, in 1972, 1974, and 1977, respectively.

Upon graduation, he worked briefly in the Electromagnetic Laboratory, University of Illinois at Urbana-Champaign. He returned to Hong Kong in 1978, and began his teaching career at the Hong Kong Polytechnic University. He joined the newly established City University of Hong Kong, Kowloon, Hong Kong, in 1984, and was instrumental in setting up a new academic department. In 1989, he was promoted to Full Professor and, in 1984, was appointed one of the first two personal chairs. He currently heads the Department of Electronic Engineering. He also heads the Wireless Communications Research Center, which he founded in 1993. He remains active in frontline research in microwave devices and antenna design for wireless communications, and has been the principal investigator of many research projects. He has authored over 200 papers, including 60 published in international journals.

Ru Shan Chen (M'93) was born in Jiangsu, China. He received the B.Sc. and M.Sc. degrees in radio engineering from Southeast University, Nanjing, China, in 1987 and 1990, respectively.

Upon graduation, he joined the Department of Electrical Engineering, Southeast University, as a Lecturer in 1995, and an Associate Professor in 1996. He is currently with the Department of Electronic Engineering, City University of Hong Kong, Kowloon, Hong Kong, where he was first a Senior Research Associate and is now a Research Fellow. He has authored over 60 academic papers in various journals and conferences. His current research interests include microwave/millimeter-wave systems, antenna, active, and passive devices, and computational electromagnetic theory.

Mr. Chen received the 1992 Third-Class Science and Technology Advance Prize awarded by the National Military Industry Department of China, the 1993 Third-Class Science and Technology Advance Prize awarded by the National Education Committee of China, and the 1996 Second-Class Science and Technology Advance Prize awarded by the National Education Committee of China. He was also the recipient of the NUST Excellent Young Teacher Prize in 1994, 1996, and 1997, respectively.

Ke Wu (M'87–SM'92) was born in Liyang, Jiangsu Province, China, on December 9, 1962. He received the B.Sc. degree (with distinction) in radio engineering from the Nanjing Institute of Technology (now Southeast University), Nanjing, China, and the D.E.A. and Ph.D. degrees (with distinction) in optics, optoelectronics, and microwave engineering from the Institut National Polytechnique de Grenoble (INPG), Grenoble, France, in 1984 and 1987, respectively.

He conducted research in the Laboratoire d'Electromagnetisme, Microondes et Optolectronics (LEMO), Grenoble, France, prior to joining the Department of Electrical and Computer Engineering, University of Victoria, B.C., Canada. He then joined the Departement de Genie Electrique et de Genie Informatique, Ecole Polytechnique de Montréal, Montréal, P.Q., Canada, as an Assistant Professor, and is currently a Full Professor. He held a 1995 Visiting Professorship jointly sponsored by the French/Quebec Governments in France, and a Visiting Professorship at the City University of Hong Kong from 1996 to 1997. He provides consulting services to a number of industries and government agencies. He is also the Head of the FCAR Research Group, and has directed a number of international collaborative research programs. He has published over 210 referred journal and conference papers and several book chapters. His current research interests include the study of three-dimensional (3-D) hybrid/monolithic planar and nonplanar integration technology, passive and active dual-mode filters, nonlinear transmission-line technology, advanced field-theory-based computer-aided design (CAD) and modeling techniques, high-frequency material characterization, and development of low-cost RF and millimeter-wave transceivers. He is also interested in modeling and design of microwave photonics, with an emphasis on traveling-wave devices. He was Chairperson of the 1996 ANTEM's Publicity Committee, and Vice-Chairperson of the Technical Program Committee (TPC) for the 1997 Asia–Pacific Microwave Conference (APMC'97). He serves on the FCAR Grant Selection Committee (1993–1996, 1998–1999), and the ISRAMT International Advisory Committee. He has served on the TPC for the TELSIKS'97 and ISRAMT'97. He also holds an Honorary Visiting Professorship at Southeast University.

Dr. Wu received a URSI Young Scientist Award, the Institution of Electrical Engineer (IEE), Oliver Lodge Premium Award, and the Asia–Pacific Microwave Prize Award. He has served on the editorial or review boards of various technical journals, including the IEEE TRANSACTIONS ON MICROWAVE THEORY AND TECHNIQUES, IEEE TRANSACTIONS ON ANTENNAS AND PROPAGATION, and the IEEE MICROWAVE AND GUIDED WAVE LETTERS. He served on the 1996 IEEE Admission and Advancement (A&A) Committee, the Steering Committee for the 1997 Joint IEEE AP-S/URSI International Symposium. He has also served as TPC member for the IEEE MTT-S International Microwave Symposium.

Dao Xiang Wang, photograph and biography not available at the time of publication.